

Numerical Modeling of Transport Properties and Comparison to Laboratory Measurements

Xin Zhan¹, Larry Schwartz², Dale Morgan¹, Wave Smith², Nafi Toksöz¹

¹ Earth Resources Laboratory, Department of Earth, Atmospheric and Planetary Sciences

Massachusetts Institute of Technology, Cambridge, MA, 02139

² Schlumberger – Doll Research, Cambridge, MA, 02139

June 10, 2008

Abstract

Transport properties, such as permeability and electrical conductivity, are important in many geophysical and petroleum applications. The microstructure of a porous medium and physical characteristics of the solid and the fluids that occupy the pore space determine the macroscopic transport properties of the medium. The computation of macroscopic properties from the rock microtomography is becoming an increasingly studied topic. The transport properties are especially difficult to determine at the microscopic scale. The purpose of this paper is to test the applicabilities to numerically calculate the geometrical and transport properties (electrical conductivity, permeability, specific surface area and surface conductivity) of porous, permeable rocks, given the digital CT microtomography images. To better address the relationship between geometrical properties and transport properties, we use a number of artificial low, medium- to high-porosity Finney's (1970) sphere packs. Numerically calculated transport properties are compared with analytical and empirical equations on the Finney pack. In particular, numerically computed permeability on the Finney pack agrees well with the permeability calculated from the computed formation factor using an empirical relationship on the same structure. This illustrates the consistence of resolving different transport properties on the same structure and the possibility of multiphysics coupling in the future. We also apply all the numerical simulations on the 3D X-ray microtomography of 23.6% porosity Berea Sandstone with 2.8 micron resolution. Numerical calculations of electrical conductivity, permeability and specific surface area on mm³ image will be compared to the laboratory measurements with those parameters on cm³ core samples. The upscaling issue will be discussed when we compare the numerical results with laboratory measurements at a different scale. We also analyze the image resolution impact on different properties to better understand the discrepancy between numerical computations and laboratory measurements. This paper provides a complete work on the numerical simulations on different physics at different scales. Numerical calculations are compared with analytic, empirical rock physics equations and laboratory measurements.

1. Introduction

Recently, computation of permeability (Alder et al., 1990; Pal et al., 2002; Ayako et al., 2006) and

electric conductivity (Alder et al., 1992; Arns et al., 2002; Pal et al., 2002) on 3D X-ray microtomography have been increasingly studied. However, complex pore geometry makes modeling and simulation of transport properties in porous media a difficult problem.

In this paper, we adopt a finite difference (FD) scheme to numerically solve the Laplace equation for the electrical problem and Stokes equation for the hydraulic problem. For effective conductivity calculation for a random medium, the three most popular numerical methods currently are finite difference (FD), finite element (FEM), and random walk (Schwartz and Banavar, 1989). To numerically solve the Navier-Stokes equation or Stokes equation, good candidates include FD, FEM and Lattice Boltzmann (LB). We have the in-house ability to solve the hydraulic problem using all three different methods. Here, we choose FD to solve two different PDEs on the same structure. There are two reasons for using FD. First, we need to know the field distribution everywhere within the structure, which eliminates the random walk method. Second, we want to carry out multiphysics coupling on the same numerical frame, which eliminates the LB method. Also we may need to couple Maxwell equation and Navier-Stokes equation on the micro-structure for the electrokinetic coupling problem (Pride et al., 1991) in the future.

We analyze the electrical conductivity, permeability, and specific surface area computation with a synthetic porous medium composed of uniform radius spheres. Spherical packing is simple in geometry and also a good representation of real rock. The radius of spherical packing could be uniformly increased to simulate different geological processes, producing granular porous media with different porosities. Many analytical, empirical rock physics models can be deduced from spherical packing, which could be applied to benchmark the numerical computation of electrical conductivity, permeability, and specific surface area. Those empirical relationships could also help us to better understand the relationship between porosity and transport property, as well as the relationship between different transport properties.

Our numerical calculations will be continued on a 23.6% Berea Sandstone 3D microtomography. Computation of electrical conductivity on the microtomography of sandstones is well studied (Arns et al., 2002). Permeability calculation using a digital rock approach is also well studied (Ayako, 2004). But minimal work has been done to estimate two transport properties on the same structure simultaneously. In particular, the permeability-conductivity relationship, which involves pore volume to surface area ratio, could also be established in our numerical calculation. By calculating all different transport properties and geometrical properties on the same structure, a good consistency between different transport properties is illustrated.

In the end, the impact of image resolution on all different transport geometrical properties is also studied. The discrete representation of continuous objects can always cause discrepancy between numerical estimation and laboratory measurements. We downscale a Finney pack of 18.5% porosity from a 200^3 cube with resolution of L , to a 25^3 cube with resolution of $8L$. The fractional changes in different parameters are calculated. Electrical conductivity is the most impacted property and the explanation for this will be provided in the paper.

2. Finite Difference Implementation for Electrical and Hydraulic Flow Simulation

The effective dc conductivity of a random material can be solved by Ohm's Law,

$$\vec{J}(r) = \sigma(r)\vec{E}(r). \quad (1)$$

The conductivity value σ of a composite n-phase material is a function of location r . For a steady state conductivity problem, where the currents are steady in time, the charge conservation equation,

$$\nabla \cdot \vec{J} + \frac{\partial \rho}{\partial t} = 0 \quad (2)$$

reduces to

$$\vec{\nabla} \cdot \vec{J}(r) = -\vec{\nabla} \cdot (\sigma(r) \cdot \vec{\nabla} V(r)) = 0. \quad (3)$$

Between phases having different conductivities, the boundary conditions require that the current density normal to the interface and the potential are continuous. We can calculate the macroscopic conductivity of the random material by applying an electric potential gradient across the sample. The volume averaged current density can be used to compute the effective conductivity from Ohm's law, as given in equation (1).

Permeability is a measure of the resistance to fluid flow under a pressure gradient of a given porous medium. The mechanism of fluid flow is given by the Navier-Stokes equation:

$$\frac{d}{dt}(\rho u) + \nabla \cdot (\rho u u) = -\nabla P + \eta \nabla^2 u, \quad (4)$$

where ρ is density, u is velocity, ∇P is pressure gradient and η is the dynamic viscosity of the fluid. For the case of laminar (slow, incompressible) flow, the fluid flow can be conveniently described by the linear Stokes equations:

$$\eta \nabla^2 \vec{u}(r) = \nabla P(r), \quad (5)$$

$$\nabla \cdot \vec{u}(r) = 0, \quad (6)$$

where u and P are the local velocity vector and pressure fields at position \vec{r} . We can calculate the macroscopic permeability of the porous medium by applying a potential gradient across the sample. The permeability, κ , of the porous medium is calculated by volume averaging the local fluid velocity (in the direction of the flow) and applying the Darcy equation:

$$u = -\frac{\kappa}{\eta} \frac{\Delta P}{L} \quad (7)$$

where u is the average fluid velocity in the direction of the flow for the porous media and L is the length of the sample porous medium across which there is an applied pressure gradient of ΔP .

To calculate the dc effective conductivity of the porous medium, we employ a finite difference (FD) scheme. The FD code solves the Laplace equation with given boundary conditions using a conjugate gradient solver (Garboczi, 1998). As for the material properties, finite difference electrical conductivity programs can handle arbitrary diagonal conductivity tensors. The intrinsic challenge of solving Laplace's equation of high contrast conductivity value for neighboring grids is overcome by adopting a gradual relaxation method. For our specific problem, the solid matrix defined to be quartz and saturation fluid can have a conductivity contrast of 7-15 orders in magnitude. To solve the

hydraulic problem, there are a few numerical approaches, including finite difference (FD), finite element (FEM) and lattice boltzmann (LB). The FD stokes solver is modified based on an industry standard finite difference (FD) code developed at NIST (National Institute of Standards and Technology, Gaithersburg, MD 20899-8621, U.S.A). We tested all three different methods on a 2D thin SEM image of San Gregorio Beach sand. The results of all three methods are in good consistence, but each has its own benefits and drawbacks. In this paper, we decide to adopt the finite difference (FD) scheme. The ultimate goal is to achieve multiphysics coupling on the micro-structure. Thus, we would like to use the same scheme to solve different physics and testify the consistency between them. We could obtain the velocity field $u(r)$ and electric field $E(r)$ at the same location within the micro-structure, which provides us the possibility of studying coupling problems, such as electrokinetic coupling, in the future.

3. Numerical Calculation of Conductivity, Permeability on Spherical Packing with Comparison to Empirical Rock Physics Model

We first performed electrical conductivity and permeability calculation on a synthetic porous medium comprised of equal spheres. Finney (1970) constructed such a packing and measured the spatial coordinates of sphere centers. The applicability of constructing granular media from Finney pack to simulate certain geological processes (grain packing, compaction, and grain growth) has been well verified (Roberts and Schwartz, 1985).

We start from the original Finney pack, which has 36.2% porosity and spheres that are just touching each other. By uniformly increasing the radius of the spheres in the packing without altering the location of the sphere centers, we could generate a series of granular porous media with a wide spectrum of porosity from 4.02% to 36.2%. In total, fourteen different porosity packings are produced, with porosities of 4.02%, 6.24%, 7.85%, 9.91%, 12.54%, 15.79%, 19.80%, 22.32%, 24.16%, 25.13%, 26.12%, 28.02%, 31.52%, and 36.2%, respectively. When the size of the sampling cube in the Finney pack exceeds four-grain radii, the fluctuation in both porosity and permeability is negligible (Ayako et al., 2006). To reduce the computation cost, we took a sampling cube of 5-grain radii in the middle of the Finney pack for our calculation.

Both electrical conductivity and permeability are calculated on our 14 granular packing using the finite difference method described above. For the electrical conductivity calculation, we assign the quartz conductivity of 10^{-14} S/m for the grain and saturated electrolyte conductivity σ_0 of 1S/m for the pore space. Formation factor, which is defined as the ratio $\sigma_0 / \sigma_{\text{eff}}$, are plotted for different porosities packing in Figure 1.

All the permeabilities of the packing after grain growth are normalized by the permeability of the original packing, denoted as κ_0 . Figure 2 shows the permeability of this class of granular media as a function of porosity. The Kozeny-Carman relationship of porosity-permeability (Carman, 1961), including the percolation threshold (Mavko and Nur, 1997), is expressed as:

$$\kappa = \frac{1}{72} \frac{(\phi - \phi_p)^3 d^2}{[1 - (\phi - \phi_p)]^2 \tau^2}, \quad (8)$$

where κ is permeability, d is grain diameter, ϕ is porosity, ϕ_p is percolation porosity, τ is tortuosity. To calculate tortuosity τ , we could use:

$$\tau^2 = \phi F, \quad (9)$$

where F is formation factor. As for the percolation porosity ϕ_p , we know for Finney pack is about 3%.

The Kozeny-Carman curve is plotted together with the numerically computed permeability data in Figure 2. Good agreement between the FD calculation and the Kozeny-Carman relationship is obtained for the entire range of porosities.

We have calculated electrical conductivity and permeability on the same structure by solving two different physical PDEs. What we want to test next is the consistency between different transport properties on the same geometry. Since electrical conductivity is usually easier to measure in the laboratory or in situ than permeability, researchers have tried to relate permeability to electrical conductivity. Paterson, Walsh and Brace (1984) have deduced the following relationship:

$$\kappa = \frac{m^2}{\kappa_0} F^{-1}, \quad (10)$$

where k_0 is a geometrical factor, $k_0=2$ for circular pores and m is the volume to surface area ratio for connected pores. From this empirical relationship, we could see that permeability is proportional to the inverse of the formation factor. We plot the permeabilities and formation factors for our 14 granular packings in logarithm scale in Figure 3. A slope of -1 could fit the data points. Given the 3D digital representation of the spherical packing, we could compute the volume to surface area ratio on the digital image. Two different algorithms are used to search for the surface pixels of the binary image, and the results are averaged to obtain the surface area. By calculating the m on the digital images, we could calculate a permeability k_{image} with given F computed from the image. We crossplot the permeability $k_{numerical}$ computed by solving Stokes equation and k_{image} calculated from Equation 10 in Figure 4. Two kinds of calculated permeabilities are in good agreement with each other.

Until now, we have shown the applicability of the FD scheme to compute electrical conductivity and permeability from the 3D digital image of porous media. The numerically computed transport properties are in good agreement with the empirical relationship. Especially, the empirical conductivity-permeability relationship is well applied on numerically calculated conductivity and permeability.

4. Numerical Calculation of Conductivity, Permeability, Specific Surface Area on Berea Sandstone with Comparison to Laboratory Measurements

We will apply the numerical calculations on the 3D microtomography of Berea Sandstone provided by Schlumberger, Doll-Research. The 23.6% porosity core sample is digitized into a 1840^3 binary voxel with 2.8 micron resolution. We select five 400^3 sub-volumes at different locations in the total 1840^3 volume in Figure 5. Sub-volume #3 is in the middle of the total volume. Sub-volumes #1, 2, 4, and 5 are in the north-west, north-east, south-west and south-east direction of the central sub-volume, respectively, to capture the both vertical and horizontal heterogeneity. The hydraulic flux

and electrical flux of one slice in sub-volume #3 are color mapped in logarithm scale in Figure 6. The electrical flux is much larger compared with hydraulic flux at the thin and narrow pores. The porosity, formation factor, permeability, and specific surface area of five sub-volumes computed from the 3D tomography are listed in Table 1. The heterogeneity of the geometry at different locations of the core sample is reflected on all four parameters. We also calculate the mean value and the variance for those five sets of data and compare with the laboratory measurements in Table 2. The numerical computations on the mm^3 images compares well with the laboratory measurements at cm^3 core samples by taking the mean value of many sub-volumes. We also plot the logarithm of permeability against the logarithm of formation factor for five sub-volumes in Figure 6. A similar linear trend in logarithm of permeability-formation factor relationship shown in Figure 3 is observed in Figure 7.

5. Image Resolution Impact on Different Transport Properties

When we numerically compute the transport properties from the digital microtomographic image, image resolution has a large impact on all the calculation values. The microstructure defined by a digital image is already discretized and thus introduces the error due to the discrete voxels to represent continuum objects. We took an 18.5% Finney pack and resolved it by a 200^3 binary image. Then we downsampled the 200^3 cube into a 100^3 cube using majority rule. In essence, eight voxels in the 200^3 cube are smeared into one voxel in the 100^3 cube. If the number of grains is larger than the number of pores in the eight voxels, then the one voxel in the 100^3 cube is assigned to be grain and vice versa. If the number of grains is equal to the number of pores in the eight voxels, then the one voxel in the 100^3 cube is randomly assigned to be either grain or pore. The smeared images from the 200^3 cube down to a 25^3 cube are plotted in Figure 8. Additionally, the resolution of the voxel is increased from the original resolution L to $8L$. Porosity, permeability, formation factor, and specific surface area are calculated for all four different scales of the image. The fractional changes in all the parameters are plotted in Figure 9. The electrical conductivity is most affected by this process. This is expected, since using coarser grids to resolve the structure tends to describe the curved grain boundaries inaccurately and close narrow pores. Closure of the narrow pores will impact the electrical current more severely than hydraulic current. By conducting the image resolution impact analysis, we could know how large is the discretization error at different resolution levels. This is especially important when we want to use a coarser grid to resolve a physically large volume due to computation power limits.

6. Conclusions

In this paper, we numerically compute different transport properties on given digital microstructures. A uniform finite difference (FD) scheme is applied to solve the Laplace equation for the electrical problem and the Stokes equation for the Hydraulic problem. The ultimate goal is to achieve multi-physics coupling on the same computation frame. Both synthetic porous media—the Finney pack composed of uniform spheres and the 3D microtomography of Berea Sandstone—are used for computation. For the Finney pack, the exact pore structure is known and we can uniformly increase the radius of the spheres to generate granular packings of different porosities. Good agreement is achieved between numerically computed electrical conductivity and differential effective medium

theory. The permeability-porosity relationship on the numerical data also agrees with the Kozeny-Carman relationship. In particular, the numerically computed electrical conductivity and permeability on the same structure follows the empirical permeability-conductivity relationship. This proves the consistency between different transport properties computed on the same structure. More important, we apply all the numerical computations on the 23.6% porosity Berea Sandstone represented by 2.8 micron resolution binary voxels. Five different sub-volumes at different locations within the core sample are taken to compute porosity, permeability, electrical conductivity, and specific surface area. Numerically computed parameters on the mm³ compare well with the laboratory measurements on the cm³ core sample. Finally, the image resolution impact on all different transport properties is studied using majority rule. Electrical conductivity is most affected by the image resolution than other parameters.

7. Acknowledgements

Support was provided by Schlumberger. The 3D microtomography of Berea Sandstone and laboratory measurements are provided by Schlumberger–Doll Research.

References

- Alder, P.M., Jacquin, C.G. and Quiblier, J.A.: 1990, Flow in simulated porous media, *Int. J. Multiphase Flow* **16**, 691-712.
- Alder, P.M., Jacquin, C.G. and Thovert, J.F.: 1992, The formation factor of reconstructed porous media, *Water Resour. Res.* **28**, 1571-1576.
- Arns, C. H.: 2001, The influences of morphology on physical properties of reservoir rock, *Ph.D. thesis, Univ. of New South Wales*.
- Ayako, K.: 2004, Permeability evolution in sandstone: digital rock approach, *Ph.D. thesis, Stanford University*
- Ayako, K., Jack, D., Youngseuk, K., Amos, N and William B.: 2006, Permeability-porosity transforms from small sandstone fragments, *Geophysics*, **71**, P.N11-N19.
- Coles, M. E., Hazlett, R.D, Muegge, E.L. Jones, K.W., Andrews, B., Siddons, P., Peskin, A. and Soll, W.E.: 1996, Developments in synchrotron X-Ray microtomography with applications to flow in porous media, paper SPE 36531, *Proc. 1996 SPE Annual Technical Conference and Exhibition*, Denver, Oct 6-9.
- Carman, P. C.: 1961, L'écoulement des gaz à travers les milieux poreus, *Bibliothèque des Sciences et des Techniques nucléaires*, P.U.F, 52.
- Finney, J.: 1970, Random packings and the structure of the liquid state, *Proc. Roy. Soc.*, **319A**, 479.
- Garbozi, E.J.: 1998, Finite Element and Finite Difference Programs for Computing the Linear Electric and Elastic Properties of Digital Image of Random Materials, *NISTIR* **6269**.
- Hazlett, R.D.: 1995, Simulation of capillary dominated displacements in microtomographic images of reservoir rocks, *Transport in Porous Media* **20**, 21-35.
- Mavko, G and Nur, A.:1997, The effect of a percolation threshold in the Kozeny-Carman relation,

- Geophysics*, **62**, 1480-1482.
- Pal, E.R., Stig, B.: 2002, Process based reconstruction of sandstones and prediction of transport properties, *Transport in Porous Media* **46**, 311-343.
- Pride, S. R. and Morgan, R. D.: 1991, Electrokinetic dissipation induced by seismic waves, *Geophysics*, **56**, 914-925.
- Roberts, J. and Schwartz, L.: 1985, Grain Consolidation and Electrical Conductivity in Porous Media, *Physical Review B* **31**, 5990.
- Schwartz, L.M., Sen P.N and Johnson, D.L.: 1989a, Influence of rough surfaces on electrolytic conduction in porous media, *Phys. Rev. B* **40**, 2450-2458.
- Schwartz, L.M and Banavar, J.R.: 1989, Transport properties of disordered continuum systems, *Phys. Rev. B* **39**, n.16, 11965-11970.
- Walsh, J. B. and Brace, W. F.: 1984, The effect of pressure on porosity and transport properties of rock, *J.Geophy. Res*, **89**, 9425-9431.

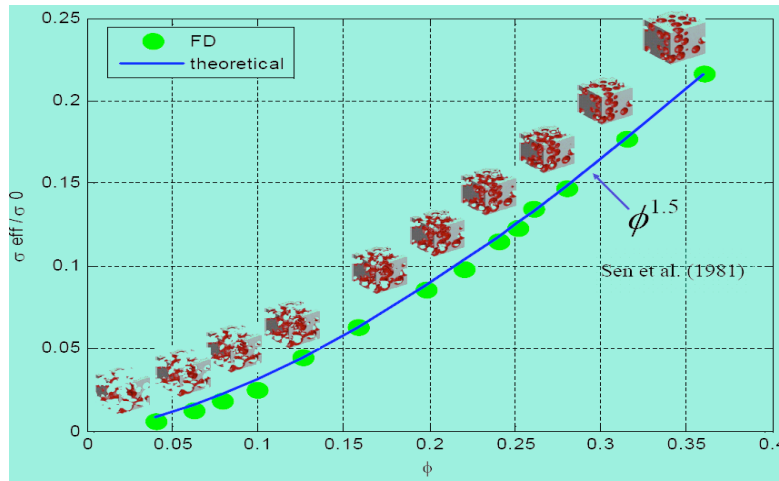


Figure 1: The ratio σ_{eff}/σ_0 as a function of porosity ϕ for 14 granular packing with porosities ranging from 4.02% to 36.2%. Green dots are the numerical results by solving Laplace equation using FD scheme. Blue curve is the differential effective medium theory by Sen et al., in 1981. The 3D pore structures of the Finney pack are also illustrated in the figure. Porosity is 36.2% when the spheres are just in contact with each other.

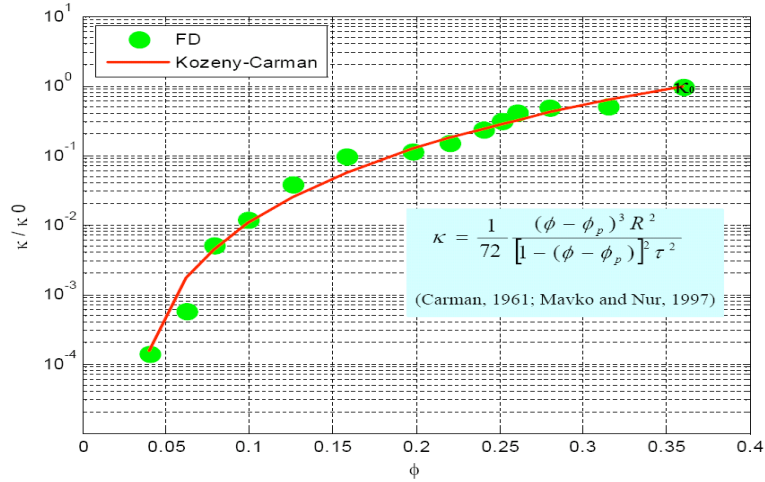


Figure 2: The normalized permeability as a function of porosity ϕ for 14 granular packing with porosities ranging from 4.02% to 36.2%. Green dots are the numerical results of solving the Stokes equation using an FD scheme. The red curve shows the Kozeny-Carman relationship.

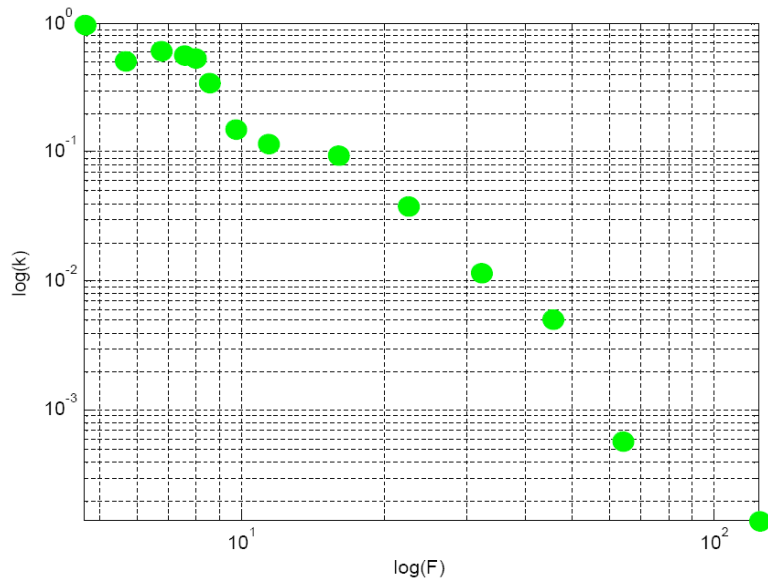


Figure 3: The logarithm of numerically calculated permeability plotted against the logarithm of numerically calculated formation factor for 14 granular packings.

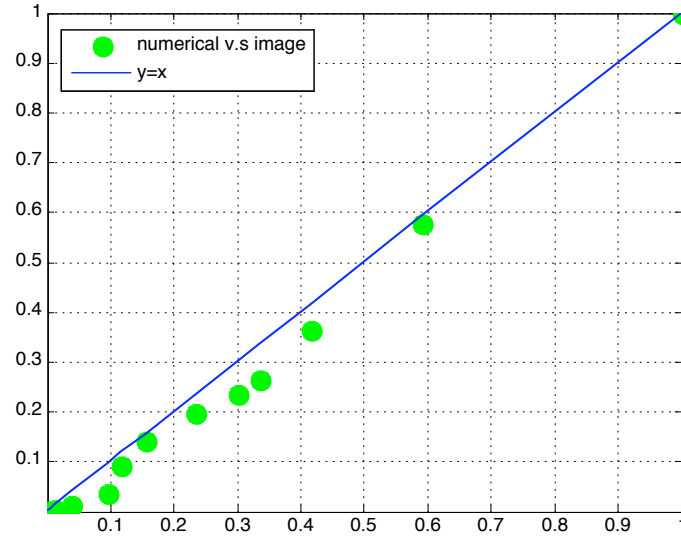


Figure 4: The cross-plot of numerically calculated permeability versus the permeability calculated from Paterson-Walsh-Brace relationship (Equation 10). Two kinds of calculated permeabilities are in good agreement with each other.

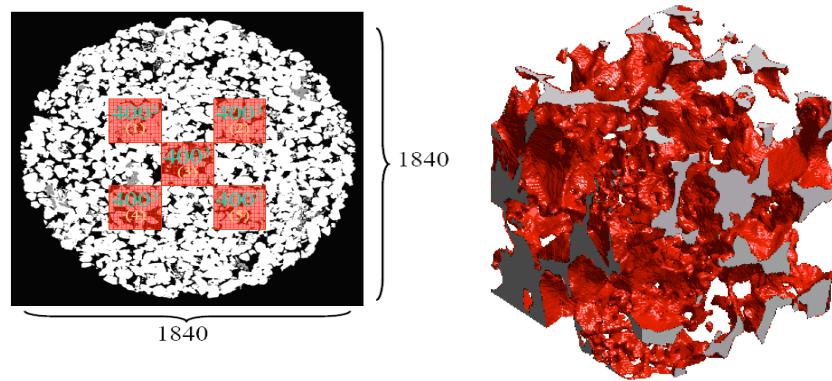


Figure 5: Selected five 400^3 sub-volumes at different locations in the total 1840^3 core sample with 2.8 micron resolution. #3 sub-volume is in the middle of the total volume. The pore cast of #3 sub-volume is shown on the left.

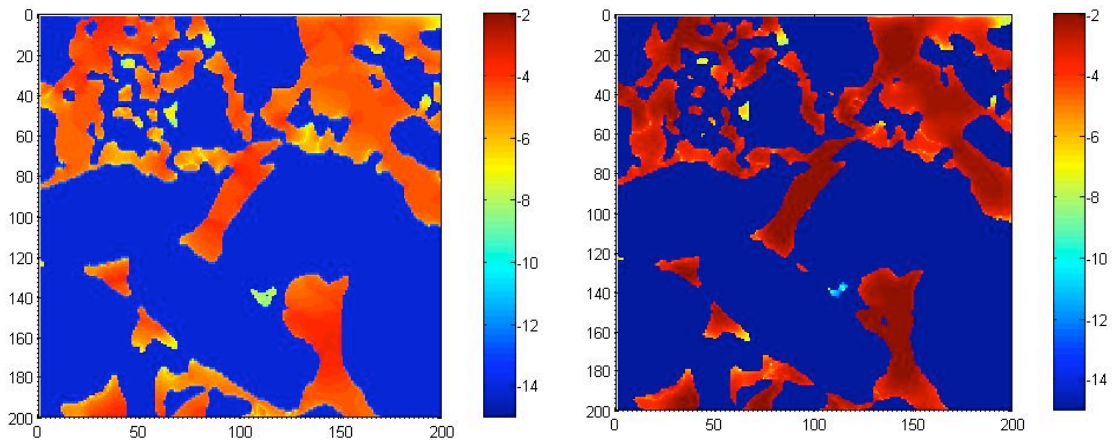
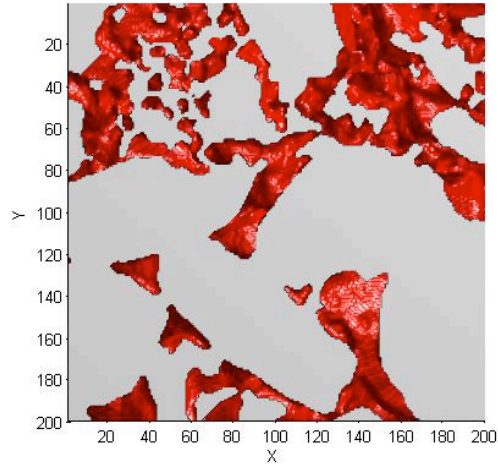


Figure 6: Electrical flux (bottom left) and hydraulic flux (bottom right) of one slice in sub-volume #3 (top) in logarithm scale.

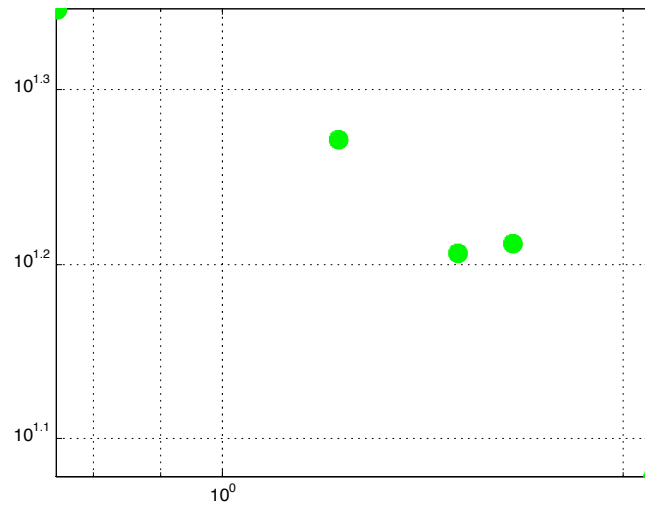


Figure 7: The logarithm of numerically calculated permeability plotted against the logarithm of numerically calculated formation factor for 5 sub-volumes in Berea Sandstone.

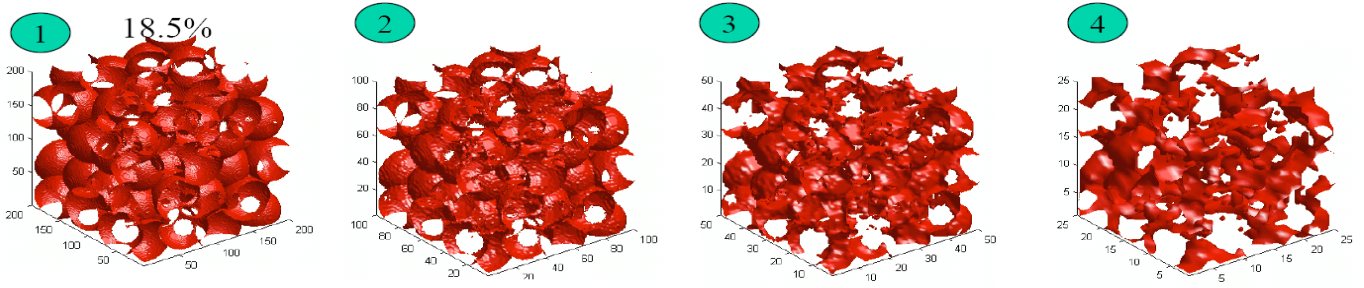


Figure 8: 18.5% porosity Finney pack resolved by a 200^3 cube and downscaled to a 50^3 cube using majority rule.

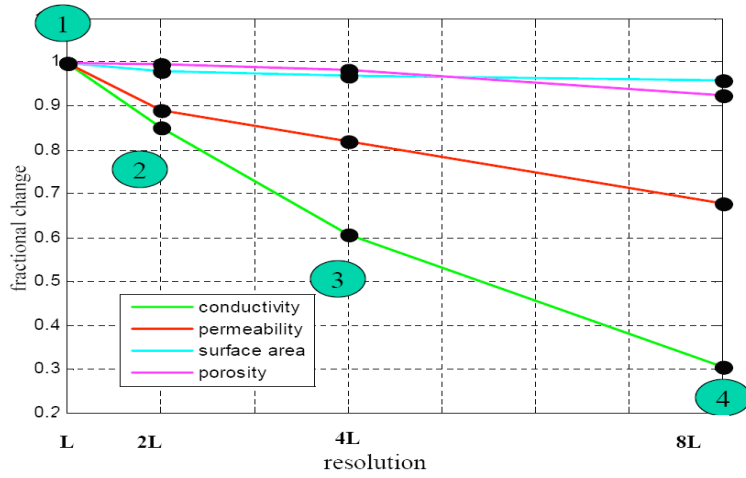


Figure 9: Fractional change in image computed porosity, electrical conductivity, permeability, and specific surface from a 200^3 cube with voxel resolution of L to a 50^3 cube with voxel resolution of $8L$.

	#1	#2	#3	#4	#5
Porosity %	22.98	23.33	23.81	24.10	23.60
Formation Factor (F)	22.23	18.69	16.11	11.98	16.31
Permeability (D)	0.75	1.22	1.50	2.10	1.65
Specific Surface Area ($e5\ m^{-1}$)	1.82	1.70	1.62	1.44	1.60

Table 1: Porosity, permeability, formation factor, and specific surface area of five selected sub-volumes (#1-#5) computed from the digital 3D microtomography.

	Lab	Numerical
Porosity %	23.56	23.64 ± 0.43
Formation Factor (F)	13.03	16.40 ± 3.76
Permeability (D)	0.90	1.23 ± 0.69
Specific Surface Area (e5 m ⁻¹)	2	1.63 ± 0.02

Table 2: Mean value and variance of different parameters for five sub-volumes and comparison with laboratory measurements.